Journal of Sound and Vibration 442 (2019) 428–444

Contents lists available at ScienceDirect

Journal of Sound and Vibration

journal homepage: www.elsevier.com/locate/jsvi

Linear disturbance observer based sliding mode control for active suspension systems with non-ideal actuator

Utkarsh S. Pusadkar, Sushant D. Chaudhari, P.D. Shendge, S.B. Phadke *

College of Engineering, Pune, India

ARTICLE INFO

Article history:
Received 8 June 2018
Revised 5 September 2018
Accepted 2 November 2018
Available online 5 November 2018
Handling Editor: J. Lam

Keywords:
Active suspension system
Actuator non-linearities
Dead-zone
Hysteresis
Disturbance observer
Sliding mode control

ABSTRACT

This paper considers the problem of designing active vehicle suspension systems in which the actuator, being affected by dead-zone and hysteresis, is non-ideal. A new method based on a disturbance observer combined with sliding mode control is proposed for compensating the effect of the actuator imperfections, uncertainties in suspension parameters and an unknown road profile. The stability of the disturbance estimator and active suspension system is proved. The performance of the scheme is assessed by simulation and experimentation on a laboratory emulation of a quarter car suspension system. The proposed controller is compared with a recently developed adaptive tracking control for active suspension system with the non-ideal actuator.

1. Introduction

Nowadays, there is a great interest in active suspension systems to improve the ride comfort in passenger cars. Designing quarter car active suspension systems is challenging because there are significant uncertainties in these systems in terms of suspension components, sprung mass and unknown road profiles. Further, the spring and damper models are often non-linear which makes the design still more challenging. Various strategies like the optimal control [1], backstepping control [2], adaptive control [3], adaptive neural network control [4], sliding mode control (SMC) [5,6], model free fractional order SMC [7], model free tracking control [8], non-linear disturbance compensator [9] to name just a few, are reported in the literature. In a large majority of the control schemes proposed, the actuator is considered to be ideal. Unfortunately, practical actuators are not ideal. They are often affected by dead-zone, hysteresis, saturation and time lags. In the absence of corrective measures, these non-idealities can degrade the performance. This paper considers the dead-zone and hysteresis non-linearities in the actuator used in active suspension systems.

A lot of work has been done on controller design for general systems with actuator imperfections like the dead-zone and backlash. Many control strategies like the adaptive control [10,11], backstepping control [12], and combinations of these methods have been proposed in the literature.

Inverse dead-zone model [13,14] has been proposed to counter the effect of dead-zone. In Refs. [15,16] adaptive and model reference control is considered for plants having dead-zone. Undesirable dead-zone is compensated using inverse dead-zone

* Corresponding author.
E-mail addresses: uspusadkar0709@gmail.com (U.S. Pusadkar), sushantchaudhari2310@gmail.com (S.D. Chaudhari), pds.instru@coep.ac.in (P.D. Shendge), sbp.instru@coep.ac.in (S.B. Phadke).

https://doi.org/10.1016/j.jsv.2018.11.003
0022-460X/

model [15]. Inverse dead-zone model is constructed by representing the unknown dead zone by a bounded disturbance and a time-varying gain. The model inversion methods work best when the model of the actuator non-linearity is perfectly known. The hysteresis non-linearity can destabilize a system [14] and must be compensated for when it is significant. The effect of hysteresis on mechanical systems is considered in Refs. [17,18]. Although the problem of non-ideal actuator is addressed in the literature via several methods, the application of linear or non-linear disturbance observer is not seen. It is shown later in this paper, that application of disturbance observer can compensate the actuator non-idealities with remarkable simplicity.

As far as the application of these methods to active suspension is concerned, one finds only a few results. In Ref. [19], a unified framework for considering dead-zone and hysteresis is proposed without requiring any prior knowledge of the dead-zone or the hysteresis parameters and then an adaptive tracking control (ATC) is designed to compensate the effect of dead-zone and hysteresis. This method avoids the need to get actuator output inverse or exact values of suspension parameters through several on-line adaptations.

The proposed scheme is motivated by Ref. [19] but uses a very different approach. The proposed scheme estimates the effect of all uncertainties and non-ideal actuator and nullifies it by using the opposite of the estimate in control. No knowledge regarding the uncertainties or their bounds is required. The estimation of uncertainties is accomplished using a linear disturbance observer and then the control combines it with sliding mode control. Therefore, the scheme is named as linear disturbance observer based sliding mode control (LDO-SMC). In Ref. [19], the problem is solved using a backstepping approach. Such an approach requires derivative of the virtual control which is not easy to obtain. In Ref. [19], the derivative of the virtual control is obtained by numerical differentiation which can result in noise amplification. The proposed strategy does away with the need for backstepping and consequently for the derivative of the virtual control. In Ref. [19], the uncertain suspension parameters and sprung mass are estimated individually. This requires four sensors for measurement of positions and velocities of the sprung and unsprung masses and involves six real-time integrations for parameter adaptation making the controller implementation costly and complex.

Main features of the proposed control are:

(a) individual estimation of uncertain parameters is not required.
(b) no knowledge of the width or slope of dead-zone and the shape or amplitude of hysteresis is required.
(c) no knowledge of road profile is required whereby the need for road preview sensors is avoided.
(d) the displacement and velocity of the unsprung mass are not required resulting in saving of two more sensors.
(e) the controller requires only one real-time integration reducing the controller complexity considerably.

Rest of the paper is organized as follows: The problem statement is given in Section 2, followed by the description of LDO-SMC in Section 3. The Section 4 gives the stability followed by simulation in Section 5 and experimentation in Section 6. The conclusion is given in Section 7.

2. Problem statement

An active quarter car suspension system of a passenger car is illustrated in Fig. 1 where the sprung mass m_s is the mass of car body and m_{us} is the unsprung mass that is constituted by the masses of the wheel, tire, and brakes. The sprung mass is supported by the passive suspension components comprising the spring k_s, damper b_s and an active control element denoted by $N(v)$. The tire is modeled as a combination of spring and damper denoted by k_t and b_t respectively. The vertical displacements of the sprung and unsprung masses, measured with respect to their static positions, are denoted respectively by x_s and x_{us} while z_r denotes an uneven road profile.

Defining the state $x = \begin{bmatrix} x_1 & x_2 & x_3 & x_4 \end{bmatrix}^T$ where

$x_1 = x_s,\ x_2 = \dot{x}_s,\ x_3 = x_{us},\ x_4 = \dot{x}_{us}$

the equations of motion from Fig. 1 can be written as

$$\dot{x}_1 = x_2 \tag{1}$$

$$\dot{x}_2 = \frac{1}{m_s}(-f_s - f_d + N(v)) \tag{2}$$

$$\dot{x}_3 = x_4 \tag{3}$$

$$\dot{x}_4 = \frac{1}{m_{us}}(f_s + f_d - f_t - N(v)) \tag{4}$$

where f_s and f_d denote the forces produced by the spring k_s and damper b_s respectively. These forces, being non-linear in practice, are modeled as

$$f_s = k_{sl}(x_1 - x_3) + k_{snl}(x_1 - x_3)^3 \tag{5}$$

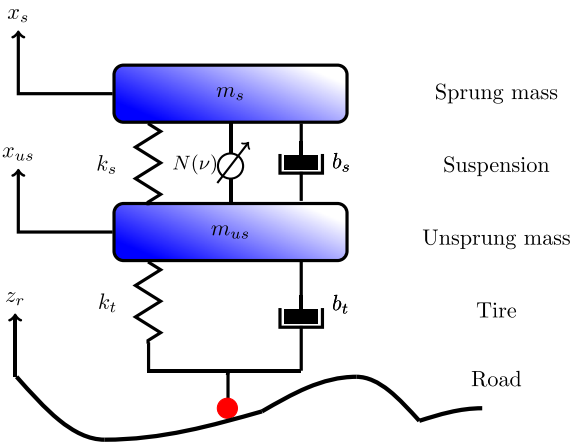

Fig. 1. Quarter car suspension system.

$$f_d = b_{sl}(x_2 - x_4) + b_{snl}(x_2 - x_4)^2 \tag{6}$$

where k_{sl}, k_{snl}, b_{sl} and b_{snl} are linear and non-linear coefficients for spring and damper respectively. The tire force denoted by f_t, is given by

$$f_t = f_{st} + f_{dt} \tag{7}$$

where

$$f_{st} = k_t(x_3 - z_r) \tag{8}$$

$$f_{dt} = b_t(x_4 - \dot{z}_r) \tag{9}$$

where k_t and b_t are tire stiffness and damping coefficients respectively. Further,

$$f_t = \begin{cases} f_{st} + f_{dt} & \text{if } k_t(x_3 - z_r) + b_t(x_4 - \dot{z}_r) < (m_s + m_{us})g \\ 0 & \text{if } k_t(x_3 - z_r) + b_t(x_4 - \dot{z}_r) \geq (m_s + m_{us})g \end{cases} \tag{10}$$

where g is acceleration due to gravity.

2.1. Non-ideal actuator

The actuator shown as $N(\nu)$ in Fig. 1 is a non-ideal actuator. It is assumed that it is affected by dead-zone or hysteresis. The force produced by the actuator is denoted as $N(\nu)$, ν being an input to the actuator. In the presence of dead-zone, the output of actuator is represented by Refs. [13,20],

$$N(\nu) = m\nu + d_d \tag{11}$$

where

$$d_d = \begin{cases} -mb_r, & \text{if } \nu \geq b_r \\ -m\nu, & \text{if } b_l < \nu < b_r \\ -mb_l, & \text{if } \nu \leq b_l \end{cases} \tag{12}$$

where m is pseudo slope of the dead-zone characteristics, $b_r > 0$ and $b_l < 0$ are unknown bounds of the dead-zone. In the presence of hysteresis, the actuator output can be modeled as in Refs. [17–19].

$$N(\nu) = \mu_1\nu + \mu_2 d_h \tag{13}$$

where $\mu_i > 0$, for$i = 1, 2$ are stiffness ratios, d_h is an auxiliary variable, expressed as

$$d_h = \dot{\nu} - \gamma|\dot{\nu}||d_h|^{n-1} - \alpha\dot{\nu}|d_h|^n, \quad d_h(0) = 0 \tag{14}$$

where γ, n and α are positive constants that control the shape and magnitude of the hysteresis loop.

As for the non-ideal actuator, dead-zone and hysteresis are only approximately known i.e., the coefficients in (11), (12), (13) and (14) are not exactly known. A unified actuator output [19] can be represented as

$$N(v) = kv + \overline{d}(v) \tag{15}$$

where $k = m$ and $\overline{d}(v) = d_d$ in case of dead-zone, while $k = \mu_1$ and $\overline{d}(v) = \mu_2 d_h$ in the case of hysteresis. A preliminary study shows that if the hysteresis and dead-zone are both present in the actuator model, the form of (15) remains unchanged. Therefore, the method proposed in this paper is likely to work without major changes.

2.2. Performance measures

The space between the sprung and unsprung masses is called the rattle space. The rattle space limit denoted by x_r is the distance between sprung and unsprung masses when the vehicle is at rest on a level ground. Relative suspension deflection (RSD), denoted by ξ, is defined as

$$\xi = \frac{x_1 - x_3}{x_r} \tag{16}$$

The relative tire force (RTF), denoted by ψ, is defined as the ratio of the dynamic tire force to the static tire force

$$\psi = \frac{f_t}{(m_s + m_{us})g} \tag{17}$$

The RSD and RTF are measures of suspension safety and road holding respectively. The magnitude of RSD must remain smaller than 1 to ensure that the rattle space limit is not violated and the magnitude of RTF must be smaller than 1 to ensure that the road holding is not lost. The measure of ride comfort is the acceleration of the sprung mass given by $\dot{x}_2$. In ISO 2631 [21], it is stated that the human body is more sensitive to acceleration in the frequency range of 4–8 Hz. The sensitivity of the human body to acceleration in this range is quantified in ISO 2631, by giving weights to frequencies in this range. A simpler way to find the weighted RMS acceleration is to pass the sprung mass acceleration signal through appropriate filters as suggested in the literature. The filter that matches the ISO 2631 ratings very closely is given in Refs. [22,23] as,

$$W(s) = \frac{87.72s^4 + 1138s^3 + 11336s^2 + 5453s + 5509}{s^5 + 92.6854s^4 + 2549.83s^3 + 25969s^2 + 81057s + 79783} \tag{18}$$

which is used in this paper.

2.3. Performance objective

The objective of the proposed control is to make the magnitude of $\dot{x}_2$ as small as possible in the presence of uncertainties and non-linearities in the suspension components, dead-zone or hysteresis in the actuator and in the absence of any knowledge about the road profile z_r. It is desirable to have the magnitudes of ξ and ψ smaller than 1 but the scope of the present paper is limited to reducing $\dot{x}_2$ as small as possible.

3. LDO-SMC

This section describes the proposed controller called LDO-SMC which is based on a linear disturbance observer used to estimate the uncertainties combined with sliding mode controller (SMC). Based on an unified actuator model from (15), the dynamic equations of the system can be written as

$$\dot{x}_1 = x_2 \tag{19}$$

$$\dot{x}_2 = \frac{1}{m_s}(-f_s - f_d + kv + \overline{d}(v)) \tag{20}$$

$$\dot{x}_3 = x_4 \tag{21}$$

$$\dot{x}_4 = \frac{1}{m_{us}}(f_s + f_d - f_t - kv - \overline{d}(v)) \tag{22}$$

It is clear that the vertical acceleration of sprung mass is a function of actual sprung mass, spring-damper coefficients, tire dynamics as well as dynamics of the actuator. In view of the uncertainty present in these coefficients, (20) is restructured by lumping the uncertainties together as

$$\dot{x}_2 = \frac{1}{m_{s0}}(-k_{s0}x_1 - b_{s0}x_2 + k_0 v) + d_1 \tag{23}$$

where m_{s0}, k_{s0}, b_{s0} and k_0 are known nominal values of m_s, k_{sl}, b_{sl} and k respectively and the lumped uncertainty d_1 is given by,

$$d_1 = \frac{1}{m_{s0}}(k_{s0}x_1 + b_{s0}x_2 - k_0 v) + \frac{1}{m_s}(-f_s - f_d + kv + \bar{d}(v)) \tag{24}$$

It can be seen from 24 that the lumped uncertainty comprises the effect of the actuator imperfections, the uncertainties in sprung mass, suspension parameters and the terms containing the unsprung mass position and velocity. Effect of the uncertainty d_1 can be nullified by estimating it and then using the opposite of the estimate in the control signal. The uncertainty is estimated using a linear disturbance observer (LDO). The parameters m_{s0} and k_0 are user chosen constants, the choice of which does not affect the control.

3.1. Design of control

Selecting a sliding surface σ as

$$\sigma = Sx_1 + x_2 \tag{25}$$

where S is a user chosen positive constant. Differentiating σ and using (19) and (23),

$$\dot{\sigma} = Sx_2 - \frac{1}{m_{s0}}(k_{s0}x_1 + b_{s0}x_2) + d_1 + \frac{k_0}{m_{s0}}v \tag{26}$$

The control v is designed by splitting it into two parts viz. v_{eq} and v_n. The component v_{eq} is used to compensate the effect of known nominal terms and v_n is used to compensate the effect of the lumped uncertainty d_1.

$$v = v_{eq} + v_n \tag{27}$$

with

$$v_{eq} = -\frac{m_{s0}}{k_0}(Sx_2 + k_1\sigma - \frac{1}{m_{s0}}(k_{s0}x_1 + b_{s0}x_2)) \tag{28}$$

$$v_n = -\frac{m_{s0}}{k_0}\hat{d}_1 \tag{29}$$

where k_1 is a user chosen positive constant and $\hat{d}_1$ is an estimate of the lumped uncertainty d_1. Using (27)–(29) in (26), $\dot{\sigma}$ works out to

$$\dot{\sigma} = -k_1\sigma + \tilde{d}_1 \tag{30}$$

where $\tilde{d}_1 = d_1 - \hat{d}_1$. The estimation of the lumped uncertainty d_1 is given in Section 3.2.

3.2. Linear disturbance observer

Let the estimate of the lumped uncertainty denoted by $\hat{d}_1$ be given by

$$\hat{d}_1 = p + w\sigma \tag{31}$$

where w is a user chosen positive constant and p is an auxiliary variable which is updated as

$$\dot{p} = -w(Sx_2 - \frac{1}{m_{s0}}(k_{s0}x_1 + b_{s0}x_2) + \hat{d}_1 + \frac{k_0}{m_{s0}}v) \tag{32}$$

Differentiating $\hat{d}_1$ and using (27), (30) and (32) we get

$$\dot{\hat{d}}_1 = w\tilde{d}_1 \tag{33}$$

Subtracting both sides of (33) from $\dot{d}_1$ gives

$$\dot{\tilde{d}}_1 = -w\tilde{d}_1 + \dot{d}_1 \tag{34}$$

The convergence of $\tilde{d}_1$ and the choice of w are discussed in Section 4. It can be seen from the control design that no knowledge of the width of the dead-zone and the shape or amplitude of the hysteresis is required. Similarly, individual estimation of uncertainties in sprung mass and suspension parameters is not required. The controller does not require displacement and velocity of the unsprung mass saving on two sensors. It can be seen that the control in LDO-SMC scheme does not need knowledge of the width, slope of dead-zone or shape, amplitude of hysteresis.

4. Stability

Consider a Lyapunov function,

$$V_1(\widetilde{d}_1) = \frac{1}{2}\widetilde{d}_1^2 \tag{35}$$

Differentiating $V_1(\widetilde{d}_1)$ and using (34) gives,

$$\dot{V}_1(\widetilde{d}_1) = \widetilde{d}_1(-w\widetilde{d}_1 + \dot{d}_1) \tag{36}$$

Assuming that the rate of change of the lumped uncertainty d_1 is bounded such that

$$|\dot{d}_1| \leqslant \beta \tag{37}$$

where β is a positive number. The assumption is reasonable for rough as well as bumpy roads which are the ones that are normally encountered. It may not hold good for roads with a step change in the road profile.

$$\dot{V}_1(\widetilde{d}_1) \leqslant -|\widetilde{d}_1|(w|\widetilde{d}_1| - \beta) \tag{38}$$

On the lines of [24], the bound on $\widetilde{d}_1$ is obtained as

$$|\widetilde{d}_1| \leqslant \lambda \tag{39}$$

where $\lambda = \frac{\beta}{w}$. It can be seen that the bound can be lowered by increasing w. Similarly, considering another Lyapunov function $V_2(\sigma) = \frac{1}{2}\sigma^2$ and using (30)

$$\dot{V}_2(\sigma) = \sigma\dot{\sigma} \tag{40}$$

$$= -k_1\sigma^2 + \widetilde{d}_1\sigma \tag{41}$$

$$\leqslant -|\sigma|(k_1|\sigma| - |\widetilde{d}_1|) \tag{42}$$

$$\leqslant -|\sigma|(k_1|\sigma| - \lambda) \tag{43}$$

The proof of ultimate boundedness given here is based on the notion of practical stability given in Ref. [24]. It can be seen from the RHS of (43), that $|\sigma|$ will be ultimately bounded and the bound is given by

$$|\sigma| \leqslant \frac{|\widetilde{d}_1|}{k_1} = \frac{\lambda}{k_1} \tag{44}$$

Thus, it is seen from (39) and (44) that σ and $\widetilde{d}_1$ are ultimately bounded [24] and their bounds can be made sufficiently small by selecting appropriate values of the estimation parameter w and the control parameter k_1.

5. Simulation results

The efficacy of the proposed control is assessed through simulation for two road profiles shown in Fig. 4. The results obtained with the proposed LDO-SMC scheme are compared with those obtained with ATC [19] for the cases when the actuator is (a) affected by dead-zone and (b) affected by hysteresis.

The parameters of the quarter car system considered are as given in Table 1.

The initial conditions of plant are taken as $x(0)\,\mathrm{T} = [0000]$. The nominal plant parameters and the control parameters are taken as $k_0 = 1$, $m_{s0} = 350$, $k_{s0} = 13500$, $b_{s0} = 1250$, $w = m_{s0} \times 900$, $k_1 = 20$ and $S = 2$. The control parameters are kept unchanged for all cases of simulation. The performance is evaluated in terms of the ride comfort, suspension deflection and ride safety as given in ISO 2631 [21] and other sources [25,26]. The evaluation of the degree of ride comfort considered here are the

Table 1
Parameters of suspension system with actuator non-linearities.

Parameter	Value	Unit	Parameter	Value	Unit
m_s	390	kg	b_{sl}	1385	$\mathrm{Nm^{-1}}s$
m_{us}	59	kg	b_{snl}	524	$\mathrm{Nm^{-2}}s^2$
k_{sl}	14500	$\mathrm{Nm^{-1}}$	k_t	190000	$\mathrm{Nm^{-1}}$
k_{snl}	160000	$\mathrm{Nm^{-3}}$	b_t	14500	$\mathrm{Nm^{-1}}s$
k	1.8	–	x_r	0.015	m
b_l	−3	–	b_r	2	–
γ	2	–	α	1	–
n	1	–	μ_2	1	–

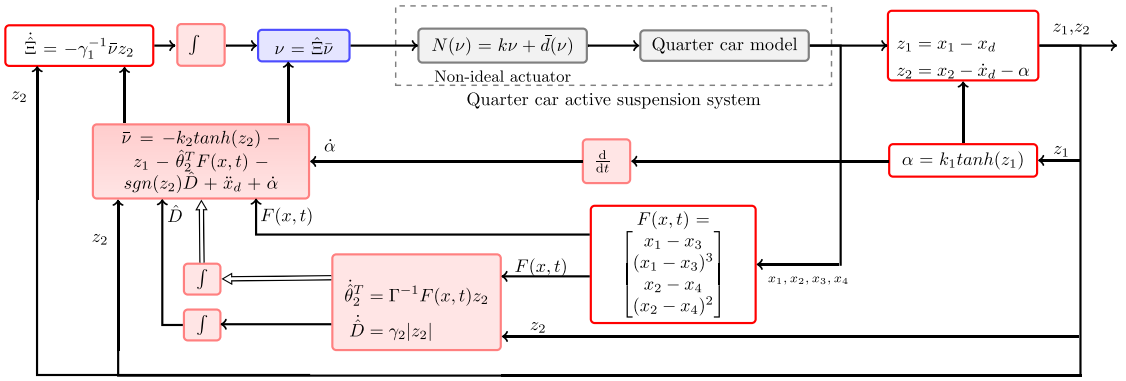

Fig. 2. Block diagram of ATC [19].

RMS and weighted RMS values of sprung mass acceleration and the RMS values of control input.

The block schematic diagram of the ATC scheme [19] is shown in Fig. 2. It can be seen that the ATC scheme requires all four states because the function $F(x, t)$ involves all four states of the sprung and unsprung masses. The number of real-time integrations in $\hat{\theta}_2$, $\hat{D}$ and $\hat{\Xi}$ is six. It can also be seen that the ATC scheme requires the derivative of the virtual control α. The block schematic of the proposed scheme is shown in Fig. 3. It can be seen that the proposed scheme requires only two states and one real-time integration for $\hat{d}_1$. The scheme is markedly simpler compared to ATC scheme.

In this study, two road profiles viz. a bump and dip profile called road profile 1 and another, an ISO class C profile called road profile 2, shown in Fig. 4(a) and (b) are considered.

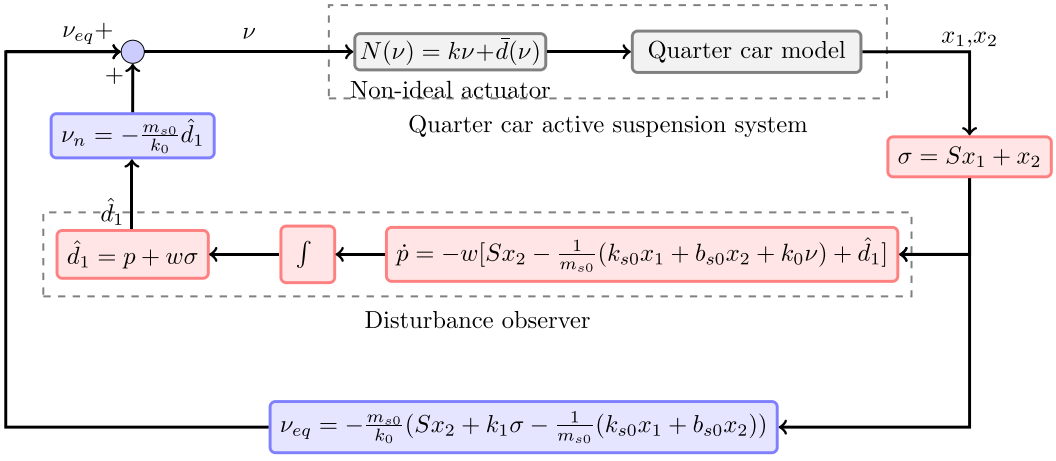

Fig. 3. Block diagram of LDO-SMC.

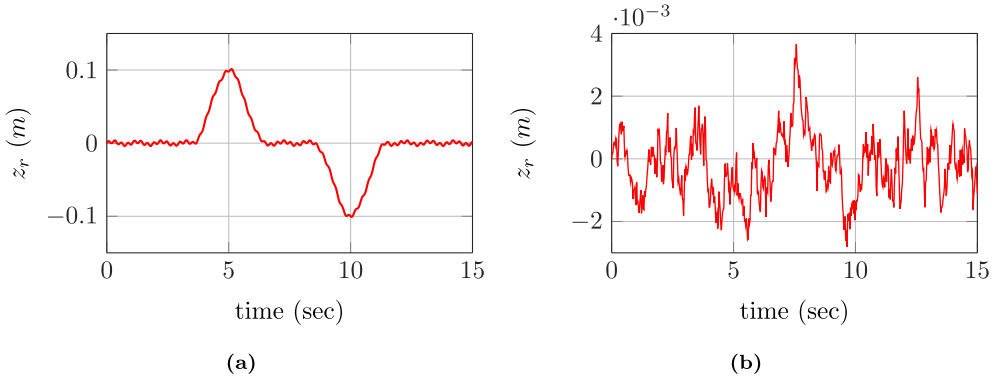

Fig. 4. Road profile z_r: (a) road profile 1 (b) road profile 2.

5.1. Case 1: road profile 1

The road profile 1 shown in Fig. 4(a) is a bump and dip profile [6] and is given by

$$z_r = \begin{cases} -0.0592t_1^3 + 0.1332t_1^2 + d(t); & 3.5 \le t < 5 \\ 0.0592t_2^3 + 0.1332t_2^2 + d(t); & 5 \le t < 6.5 \\ 0.0592t_3^3 - 0.1332t_3^2 + d(t); & 8.5 \le t < 10 \\ -0.0592t_4^3 - 0.1332t_4^2 + d(t); & 10 \le t < 11.5 \\ d(t); & else \end{cases} \tag{45}$$

where $d(t) = 0.002\sin(2\pi t) + 0.002\sin(7.5\pi t)$, is a periodic disturbance and the time intervals are described as $t_1 = t - 3.5$, $t_2 = t - 6.5$, $t_3 = t - 8.5$ and $t_4 = t - 11.5$. The responses for this road profile in the presence of dead-zone and hysteresis are shown in Figs. 5 and 6 respectively. Performance of the proposed LDO-SMC control strategy is evaluated in comparison with ATC. The acceleration of sprung mass $\dot{x}_2$, shown in Fig. 5(b), could be achieved using almost the same magnitude of control input

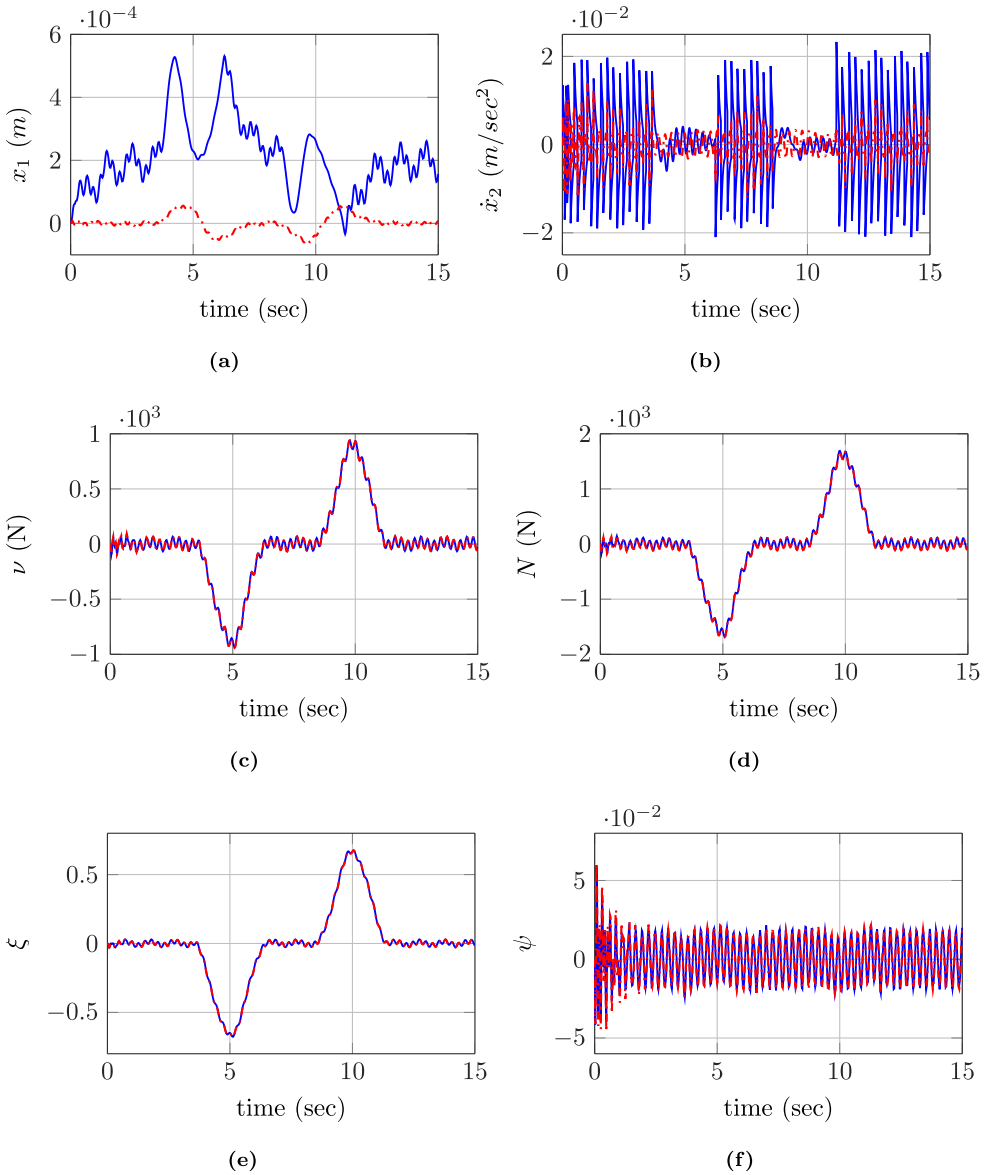

Fig. 5. Simulation results of dead-zone for road profile 1: ATC (blue) and LDO-SMC (dashed dotted red). (a) Sprung mass deflection. (b) Sprung mass acceleration. (c) Control input. (d) Actuator output. (e) RSD. (f) RTF. (For interpretation of the references to colour in this figure legend, the reader is referred to the Web version of this article.)

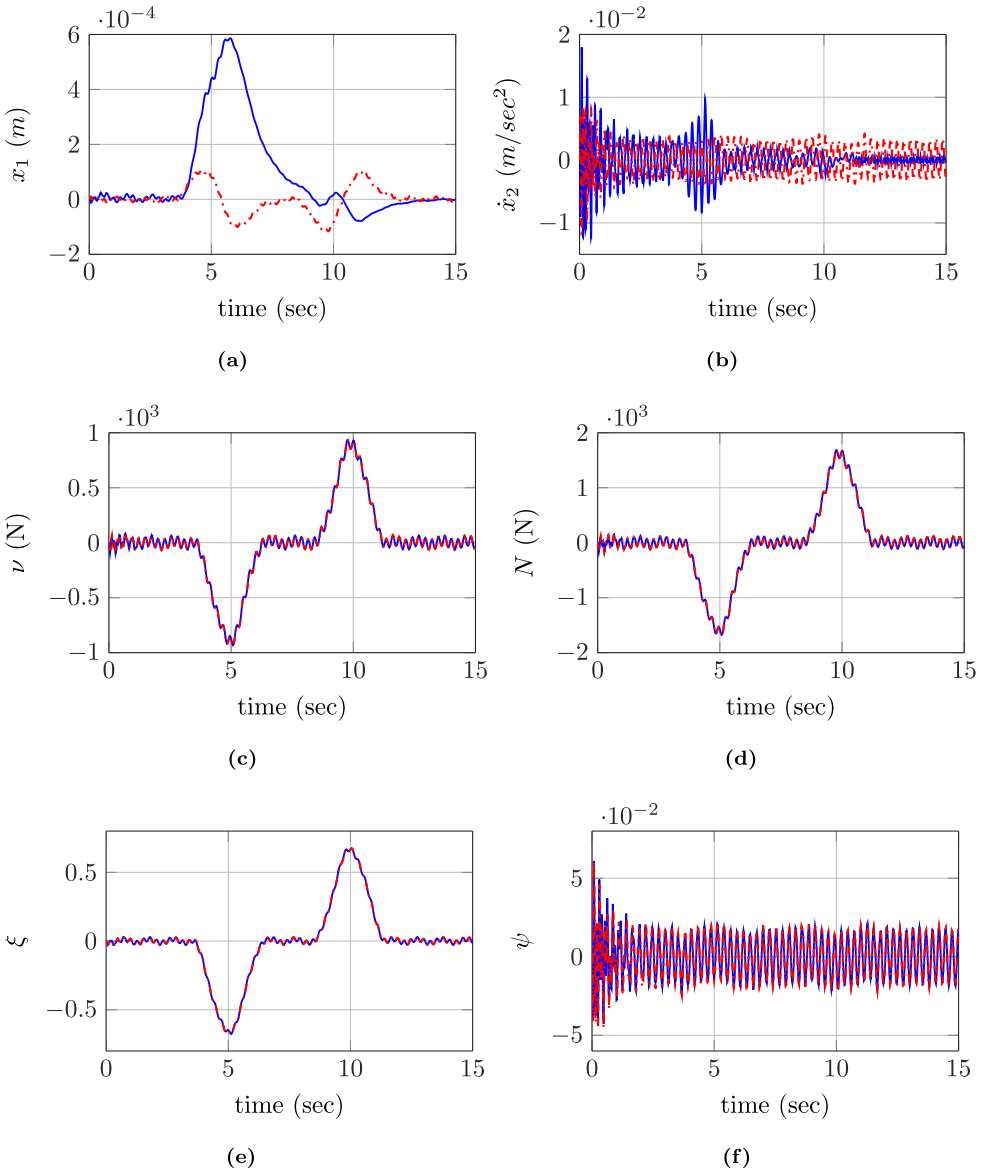

Fig. 6. Simulation results of hysteresis for road profile 1: ATC (blue) and LDO-SMC (dashed dotted red). (a) Sprung mass deflection. (b) Sprung mass acceleration. (c) Control input. (d) Actuator output. (e) RSD. (f) RTF. (For interpretation of the references to colour in this figure legend, the reader is referred to the Web version of this article.)

ν as shown in Fig. 5(c).

It is observed from Fig. 5(e) and (f), that RSD and RTF are also maintained within the limit in both schemes.

In the case of hysteresis, sprung mass displacement x_1 obtained with LDO-SMC and ATC are shown in Fig. 6(a).

The plots of the control effort, RSD and RTF are shown in Fig. 6(c), (e) and (f) respectively.

The summary of simulation results for road profile 1 based on evaluation of degree of ride comfort is given in Table 2. Full comparison with passive suspension is not shown graphically to save space but the case is included in the tabular summary and later graphical comparison with sprung mass acceleration is included.

5.2. Case 2: road profile 2

The road profile 2 is shown in Fig. 4(b). It is a class C road profile as per ISO 8608 [27] which is obtained by using the shaping filter method [28] as described below:

$$\dot{z}_r(t) = -\delta V z_r(t) + \omega(t) \tag{46}$$

Table 2
Summary of simulation results for road profile:1.

Measures		Peak $\dot{x_2}$	RMS $\dot{x_2}$	WRMS $\dot{x_2}$	Peak ν	RMS ν
Passive		0.5829	0.2233	0.1542	–	–
Dead-zone	ATC	0.0564	0.0141	0.0122	958.6982	339.4417
	LDO-SMC	0.0148	0.0027	0.0024	938.7522	340.4234
Hysteresis	ATC	0.0169	0.0025	0.0024	937.0714	338.0650
	LDO-SMC	0.0100	0.0026	0.0023	936.5675	338.9795

Measures		Peak ξ	Peak ψ	RMS ψ
Passive		0.0685	0.0528	0.0220
Dead-zone	ATC	0.6854	0.0662	0.0147
	LDO-SMC	0.6749	0.0655	0.0143
Hysteresis	ATC	0.6749	0.0641	0.0140
	LDO-SMC	0.6749	0.0654	0.0143

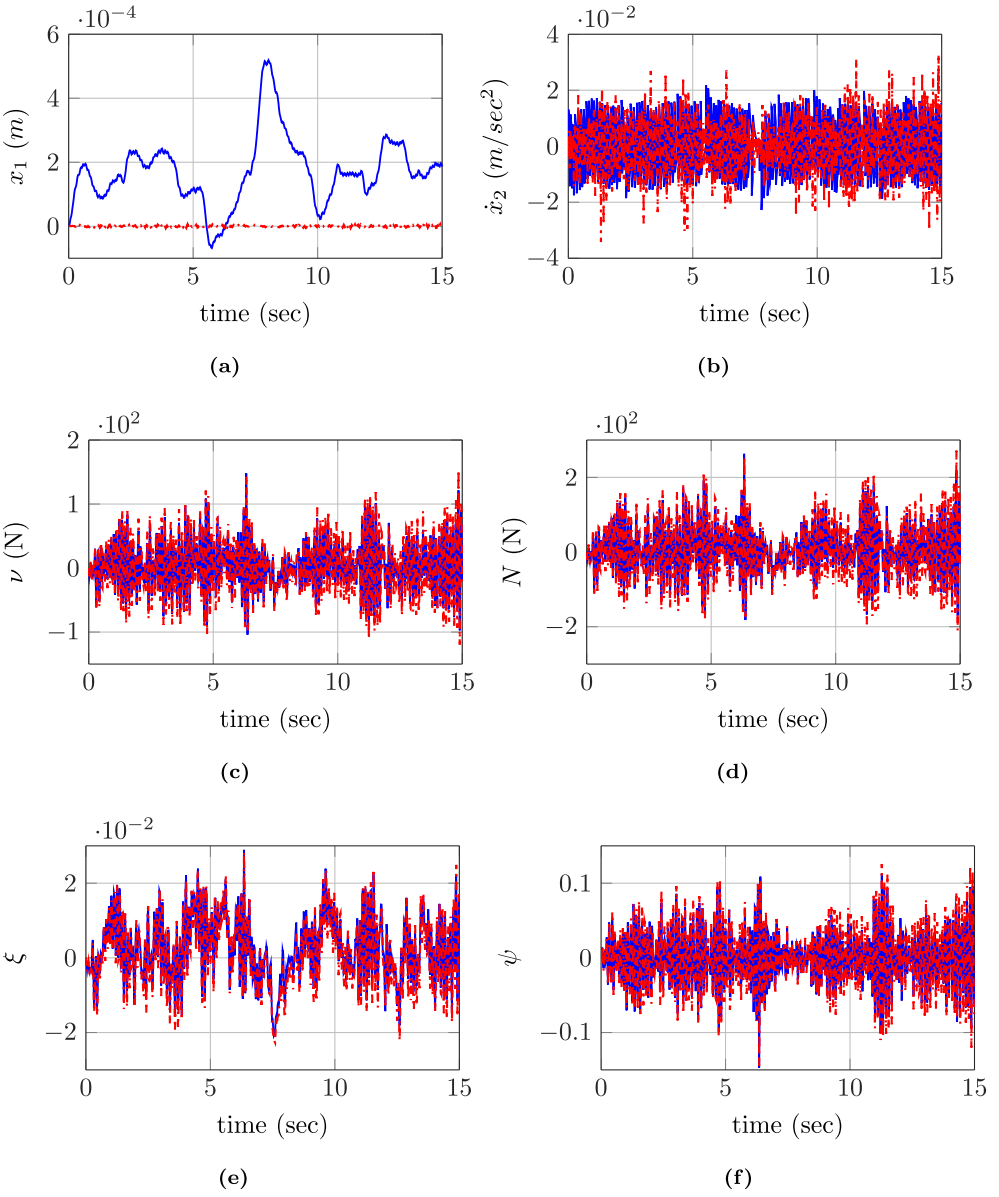

Fig. 7. Simulation results of dead-zone for road profile 2: ATC (blue) and LDO-SMC (dashed dotted red). (a) Sprung mass deflection. (b) Sprung mass acceleration. (c) Control input. (d) Actuator output. (e) RSD. (f) RTF. (For interpretation of the references to colour in this figure legend, the reader is referred to the Web version of this article.)

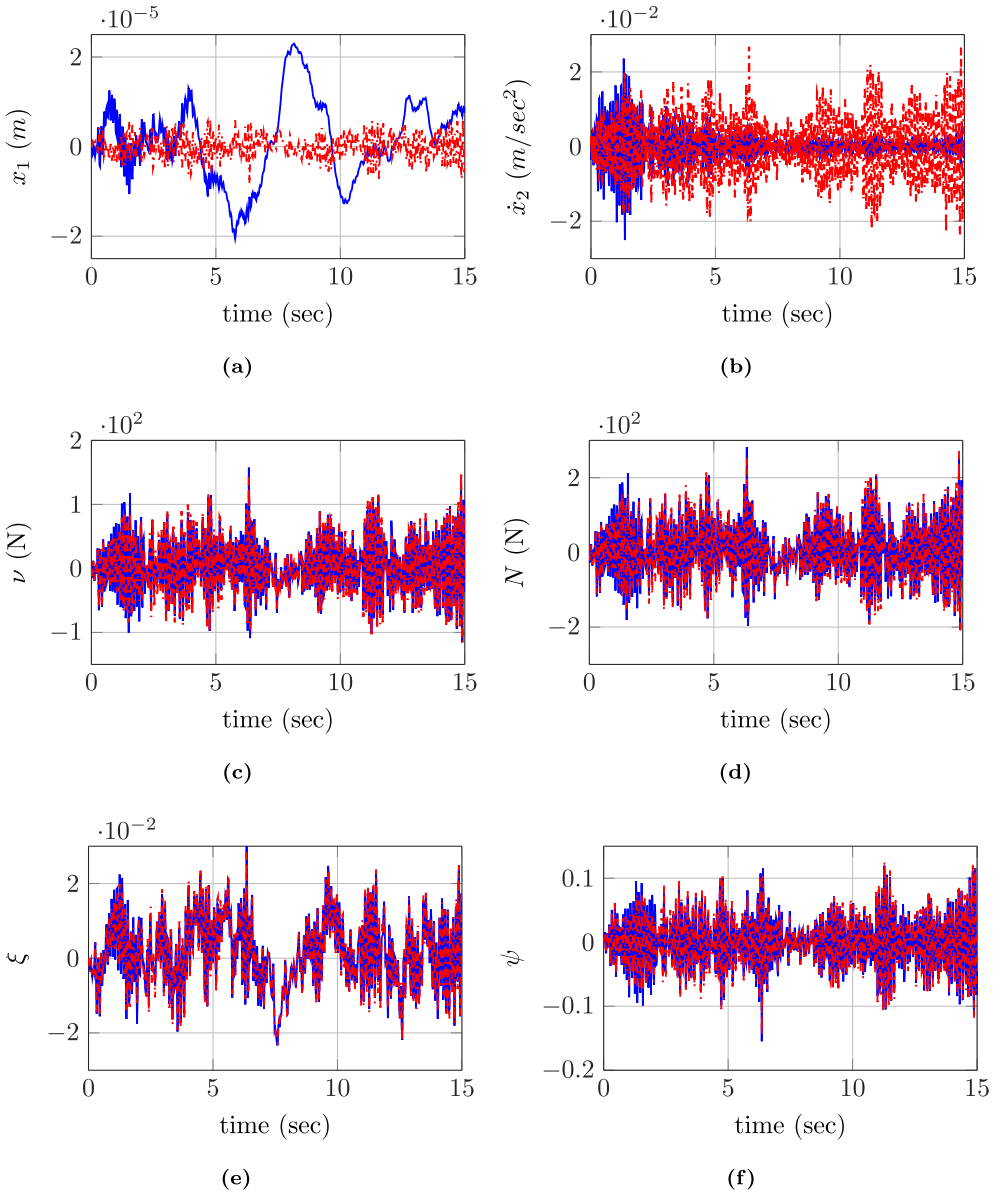

Fig. 8. Simulation results of hysteresis for road profile 2: ATC (blue) and LDO-SMC (dashed dotted red). (a) Sprung mass deflection. (b) Sprung mass acceleration. (c) Control input. (d) Actuator output. (e) RSD. (f) RTF. (For interpretation of the references to colour in this figure legend, the reader is referred to the Web version of this article.)

where V is vehicle speed, Φ_0 is value of power spectral density of excitation frequency $\omega(t)$ at the reference wave number depending upon type of road surface. Selecting $\delta = 0.127$, $\Phi_0 = 16 \times 10^{-6}\,\mathrm{m}^3$ and $V = 30\,\mathrm{m/s}$, the class C road profile is generated.

The results of simulation for this road profile with dead-zone and hysteresis are shown in Figs. 7 and 8. Table 3 summarizes the results. Full comparison with passive suspension is not shown graphically to save space but the case is included in the tabular summary.

To illustrate the effect of the control w.r.t passive suspension just the sprung mass acceleration plots for road profile 1 and 2 are shown in Figs. 9 and 10. respectively.

5.3. Discussion

It can be seen from the simulation results, that both the ATC and the proposed LDO-SMC schemes are successful in negating the effect of dead-zone and hysteresis for both road profiles. In so far as the performance is concerned, the two methods give very similar results. Since tuning of gains can improve the performance of either scheme, it is only fair to say that performance

Table 3
Summary of simulation results for road profile:2.

Measures		Peak $\dot{x}_2$	RMS $\dot{x}_2$	WRMS $\dot{x}_2$	Peak ν	RMS ν
Passive		0.2582	0.0800	0.0716	–	–
Dead-zone	ATC	0.0609	0.0149	0.0142	208.3286	58.7691
	LDO-SMC	0.0358	0.0090	0.008	161.5140	48.5716
Hysteresis	ATC	0.0137	0.0033	0.0033	65.0185	17.6453
	LDO-SMC	0.0112	0.0030	0.0030	55.5283	16.2148

Measures		Peak ξ	Peak ψ	RMS ψ
Passive		0.0147	0.0656	0.0168
Dead-zone	ATC	0.0348	0.1565	0.0521
	LDO-SMC	0.0293	0.1347	0.0494
Hysteresis	ATC	0.0116	0.0639	0.0168
	LDO-SMC	0.0112	0.0552	0.0157

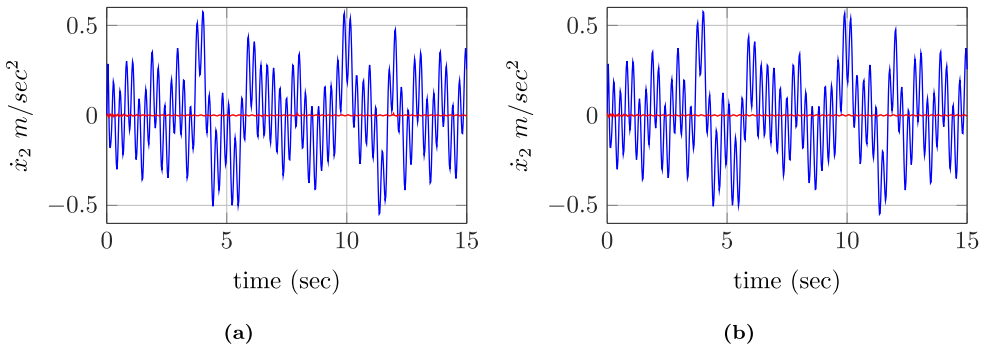

Fig. 9. Simulation results of acceleration of sprung mass for road profile 1 with passive (blue) and active controller (red): (a) Dead-zone; (b) Hysteresis. (For interpretation of the references to colour in this figure legend, the reader is referred to the Web version of this article.)

wise two schemes are equally good. However, to achieve the performance, ATC needs more real-time integrations compared to LDO-SMC and two additional state measurements. The point is emphasized through Figs. 2 and 3.

It is worth noting that the design parameters for the proposed scheme are kept unchanged for all the road profiles shown here. The performance was also assessed for some other profiles of Class D. It was found that the control strategy works very well for these road profiles as well without any change in control parameters. The plots are omitted to save space.

6. Experimental results

To investigate the effectiveness of LDO-SMC scheme on real hardware, a lab scale emulation of a quarter car suspension system shown in Fig. 11 is used [29]. The hardware mimics the sprung and unsprung masses and the road by using three plates. The blue plate representing the sprung mass has as adjustable dead weight on top. The red plate stands for the unsprung mass. The suspension spring and damper and rotary DC motor actuator are placed between the blue and red plate. A DC servo placed

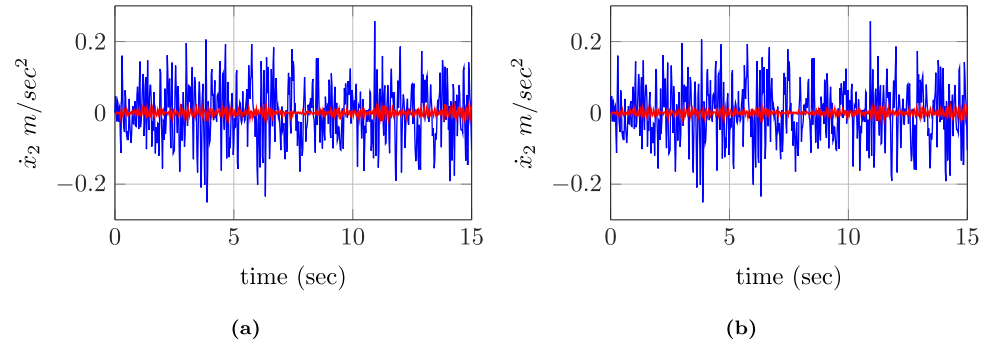

Fig. 10. Simulation results of acceleration of sprung mass for road profile 2 with passive (blue) and active controller (red): (a) Dead-zone; (b) Hysteresis. (For interpretation of the references to colour in this figure legend, the reader is referred to the Web version of this article.)

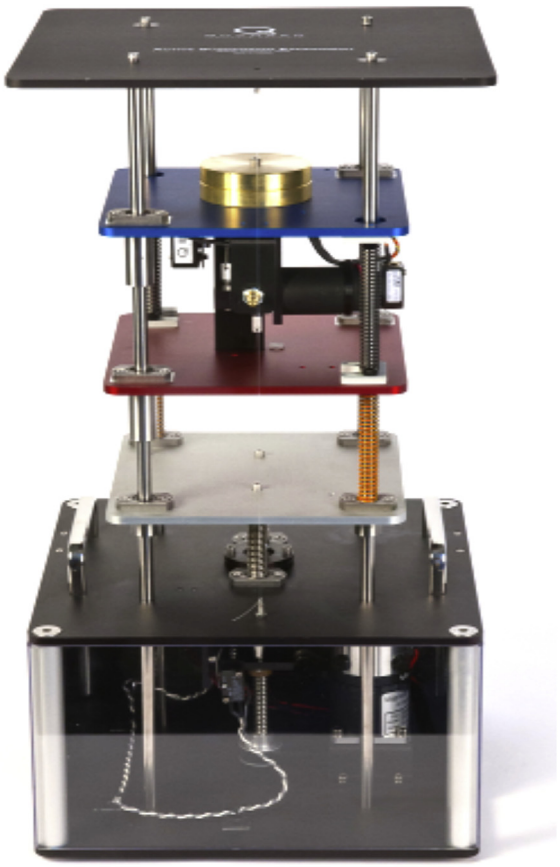

Fig. 11. Laboratory setup.

Table 4
Parameters of suspension system for hardware setup.

Parameter	Value	Unit	Parameter	Value	Unit
m_s	2.5	kg	k_t	2500	Nm^{-1}
m_{us}	1	kg	b_{us}	5	$Nm^{-1}s$
k_s	980	Nm^{-1}	k	1.8	–
b_s	7.5	$Nm^{-1}s$	x_r	0.038	m

at the bottom of the setup generates a signal to move the silver plate to imitate the uneven road profile. The position of the blue and red plates are sensed by 10-bit optical encoders while the acceleration is sensed by an accelerometer. As for the sprung mass velocity, the information is derived by passing the sprung mass position through high pass filter. It may be noted that the control designed does not require the position and velocity of the unsprung mass as well as the sprung mass acceleration. As such the control uses the measurement from only one sensor viz. the encoder to measure the position of the blue plate. The same test bench is also used in Refs. [30–34] to validate various control strategies.

The values of system parameters are given in Table 4.

The performance of active suspension system with individual dead-zone and hysteresis are assessed for road profile 3 shown in Fig. 12, which is a scaled down version of the profile in Fig. 4 (a).

The nominal plant parameters are taken as $m_{s0} = 2$, $k_{s0} = 800$, $b_{s0} = 6$, and the control parameters are selected as $w = m_{s0} \times 100$ and $S = 2$. The suspension system is given by the following equations:

$$\dot{x}_1 = x_2 \tag{47}$$

$$\dot{x}_2 = \frac{1}{m_{s0}}(-k_{s0}x_1 - b_{s0}x_2 + k_0 v) + d_1 \tag{48}$$

$$\dot{x}_3 = x_4 \tag{49}$$

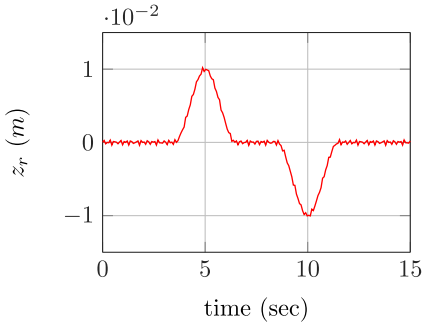

Fig. 12. Road profile 3: z_r for experimental setup.

$$\dot{x}_4 = \frac{1}{m_{us}}(f_s + f_d - f_t - N(v)) \tag{50}$$

$$f_s = k_s(x_1 - x_3), \qquad f_d = b_s(x_2 - x_4) \tag{51}$$

$$f_{st} = k_t(x_3 - z_r),\ f_{dt} = b_t(x_4 - \dot{z}_r),\ f_t = f_{st} + f_{dt} \tag{52}$$

f_s, f_d and f_t are spring, damper and tire forces respectively. No knowledge of the system parameters is assumed for the design of control. Although the test rig does not have non-ideal actuator, the non-idealities are introduced by using control logic in this paper. This approach is not uncommon, e.g. in Ref. [35] it is stated that the backlash non-linearity is introduced into experimental platform artificially.

This controller develops the control signal v which is used to generate $N(v)$, elucidated by (15) which is applied as a control input to the DC motor actuator. For dead-zone, $\overline{d}(v) = d_d$ with $m = 1.8$, $b_l = -3$ and $b_r = 2$. Similarly for hysteresis, $\overline{d}(v) = \mu_2 d_h$ with $\mu_1 = 1.8, \mu_2 = 1, \gamma = 2, \alpha = 1, n = 1$.

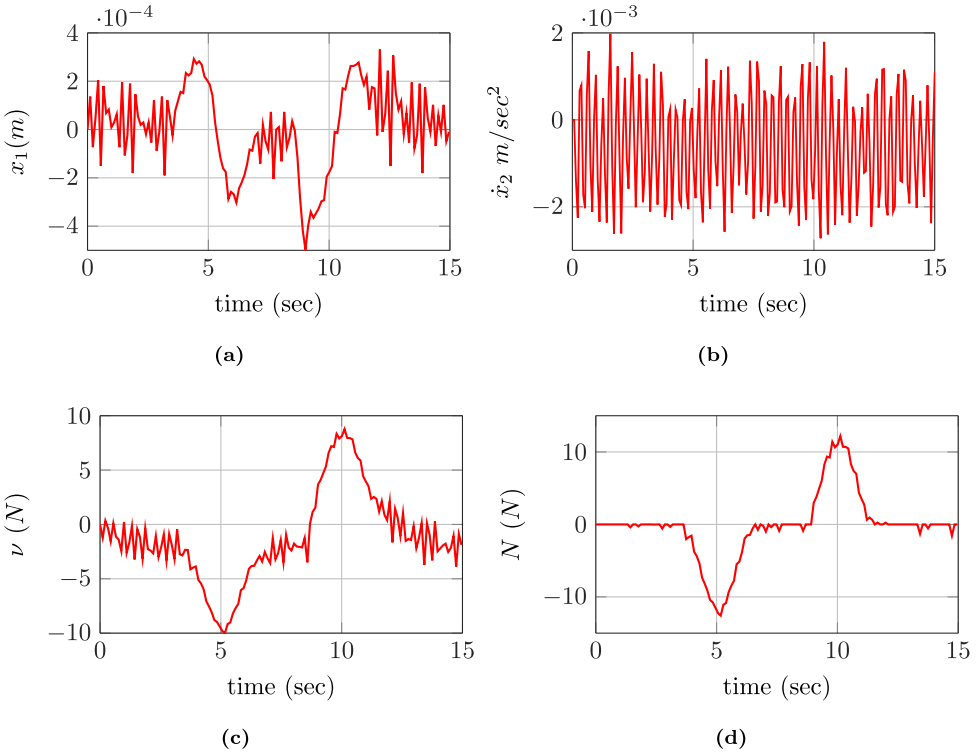

Fig. 13. Experimental results of actuator with dead-zone. (a) Sprung mass deflection. (b) sprung mass acceleration. (c) Actuator input. (d) Actuator output.

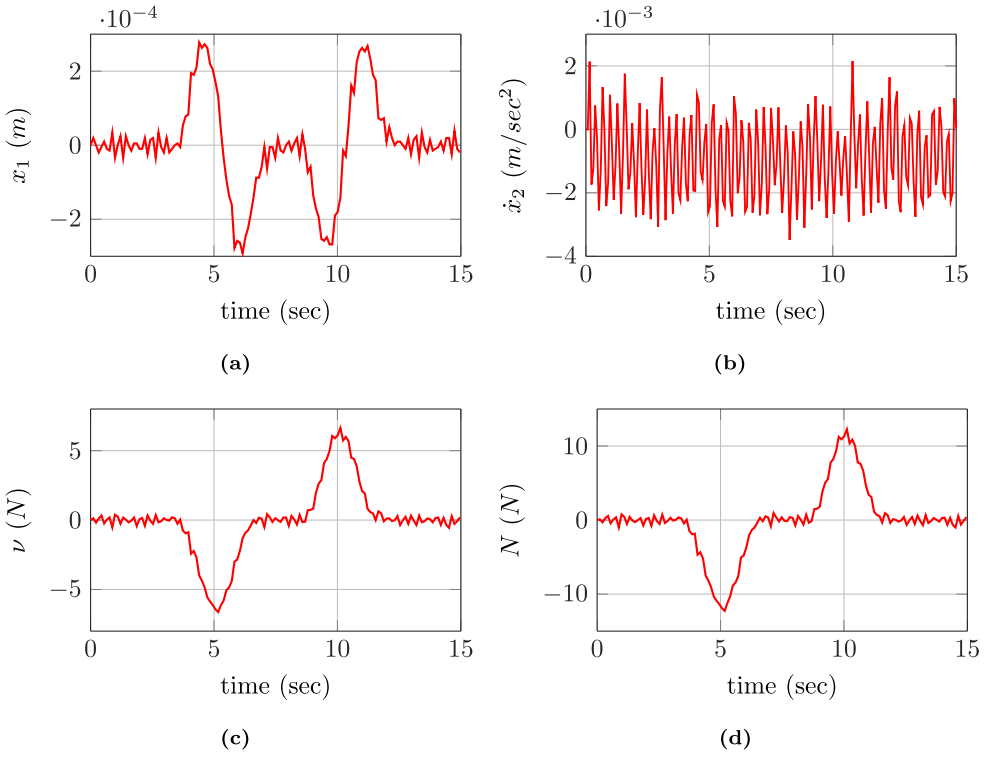

Fig. 14. Experimental results of actuator with hysteresis. (a) Sprung mass deflection. (b) sprung mass acceleration. (c) Actuator input. (d) Actuator output.

Table 5
Summary of experimental results for road profile:3.

Measures		Peak $\dot{x_2}$	RMS $\dot{x_2}$	Peak ν	RMS ν
Passive		0.2610	0.1264	–	–
Dead-zone	LDO-SMC	0.0025	0.0014	8.8204	4.2591
Hysteresis	LDO-SMC	0.0048	0.0016	6.6845	2.5092

Measures		Peak ξ	Peak ψ	RMS ψ
Passive		0.1977	0.0656	0.0437
Dead-zone	LDO-SMC	0.6746	0.1352	0.0146
Hysteresis	LDO-SMC	0.6746	0.1354	0.0146

The observations of Section 5 qualitatively hold good for the experimental results shown in Figs. 13 and 14. Based on evaluation of ride comfort Table 5 summarizes the experimental results. The comparison with passive suspension is not shown

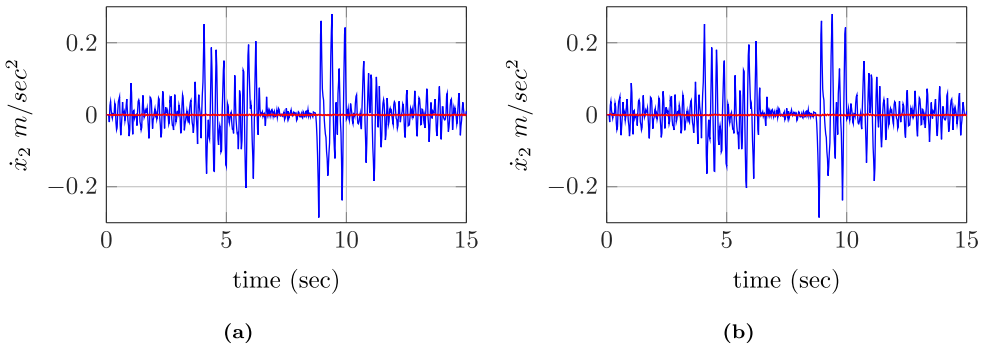

Fig. 15. Hardware result of road profile 3 with passive (blue) and active controller (red): (a) Dead-zone; (b) Hysteresis. (For interpretation of the references to colour in this figure legend, the reader is referred to the Web version of this article.)

graphically to save space but the case is included in the tabular summary. Later graphical comparison of just the sprung mass acceleration is shown. While with the consideration of non-idealities in a system, these variations are much smaller. Thus a single controller works satisfactorily for non-ideal actuator uncertainties delivering the same level of ride comfort. Comparison with passive suspension is illustrated in Fig. 15.

7. Conclusion

In this paper an LDO-SMC scheme is developed for active suspension systems in which the actuator is not ideal. The actuator affected by dead-zone and hysteresis is considered. The proposed LDO-SMC scheme successfully compensated the effect of dead-zone and hysteresis along with other uncertainties in system parameters. The control design is robust to uncertainties in the non-ideal actuator in terms of the slope and width of dead-zone and shape and amplitude of hysteresis. The proposed scheme is compared with the ATC scheme. It is found that the proposed scheme gives comparable performance with much reduced complexity and without having to use the states of the unsprung mass. Road profiles of bump and dip as well as ISO class C were considered for validation. Since the effects of non-ideal actuator and other uncertainties were compensated using a DO, the control is robust to a variety of road profiles which is confirmed by simulation and hardware results.

Acknowledgement

The authors would like to acknowledge with thanks that this work was supported by Science and Engineering Research Board, Dept of Science and Technology, Govt of India vide their sanction letter no.SB/S3/EECE/219/2016.

References

[1] D. Hrovat, Survey of advanced suspension developments and related optimal control applications, Automatica 33 (10) (1997) 1781–1817.
[2] N. Yagiz, Y. Hacioglu, Backstepping control of a vehicle with active suspensions, Contr. Eng. Pract. 16 (12) (2008) 1457–1467.
[3] G. Koch, S. Spirk, E. Pellegrini, N. Pletschen, B. Lohmann, Experimental validation of a new adaptive control approach for a hybrid suspension system, in: American Control Conference (ACC), 2011, IEEE, 2011, pp. 4580–4585.
[4] F. Zhao, S.S. Ge, F. Tu, Y. Qin, M. Dong, Adaptive neural network control for active suspension system with actuator saturation, IET Control Theory & Appl. 10 (14) (2016) 1696–1705.
[5] B. Mohan, S.B. Phadke, Variable structure active suspension system, in: Industrial Electronics, Control, and Instrumentation, 1996., Proceedings of the 1996 IEEE IECON 22nd International Conference on, vol. 3, IEEE, 1996, pp. 1945–1948.
[6] P.-C. Chen, A.-C. Huang, Adaptive sliding control of non-autonomous active suspension systems with time-varying loadings, J. Sound Vib. 282 (3) (2005) 1119–1135.
[7] H. Wang, G.I. Mustafa, Y. Tian, Model-free fractional-order sliding mode control for an active vehicle suspension system, Adv. Eng. Software 115 (2018) 452–461.
[8] W. Jue, Z. Jing, Model-free tracking control for vehicle active suspension systems, in: 34th Chinese Control Conference (CCC), IEEE, 2015, pp. 8067–8072.
[9] V.S. Deshpande, P.D. Shendge, S.B. Phadke, Dual objective active suspension system based on a novel nonlinear disturbance compensator, Veh. Syst. Dyn. 54 (9) (2016) 1269–1290.
[10] C. Hu, B. Yao, Q. Wang, Adaptive robust precision motion control of systems with unknown input dead-zones: a case study with comparative experiments, IEEE Trans. Ind. Electron. 58 (6) (2011) 2454–2464.
[11] N.J. Ahmad, H.K. Ebraheem, M.J. Alnaser, J.M. Alostath, Adaptive control of a dc motor with uncertain deadzone nonlinearity at the input, in: Control and Decision Conference (CCDC), 2011 Chinese, IEEE, 2011, pp. 4295–4299.
[12] G. Tao, A. Taware, Control by Compensation of Nonlinearities, Control Systems, Robotics and Automation-volume III: System Analysis and Control: Classical Approaches-iii, 2009, pp. 165–171.
[13] D. Recker, P. Kokotovic, D. Rhode, J. Winkelman, Adaptive nonlinear control of systems containing a deadzone, in: Decision and Control, 1991., Proceedings of the 30th IEEE Conference on, IEEE, 1991, pp. 2111–2115.
[14] J. Dong, B. Mo, The adaptive pid controller design for motor control system with backlash, in: Intelligent Control and Information Processing (ICICIP), 2013 Fourth International Conference on, IEEE, 2013, pp. 59–63.
[15] G. Tao, P.V. Kokotovic, Adaptive control of plants with unknown dead-zones, IEEE Trans. Automat. Contr. 39 (1) (1994) 59–68.
[16] T. Chang, D. Yuan, H. Hanek, Matched feedforward/model reference control of a high precision robot with dead-zone, IEEE Trans. Contr. Syst. Technol. 16 (1) (2008) 94–102.
[17] R. Bouc, Forced vibration of mechanical systems with hysteresis, in: Proceedings of the Fourth Conference on Non-linear Oscillation, Czechoslovakia, Prague, 1967, pp. 32–39.
[18] O. Solomon, Some typical shapes of hysteretic loops using the bouc-wen model, J. Inf. Syst. Oper. Manag. (2013) 1–9.
[19] H. Pan, W. Sun, X. Jing, H. Gao, J. Yao, Adaptive tracking control for active suspension systems with non-ideal actuators, J. Sound Vib. 399 (2017) 2–20.
[20] G. Tao, P.V. Kokotovic, Adaptive Control of Systems with Actuator and Sensor Nonlinearities, John Wiley & Sons, Inc., 1996.
[21] ISO-2631, Mechanical Vibration and Shock: Evaluation of Human Exposure to Whole-body Vibration Part 1, General Requirements, ISO, Geneva.
[22] L. Zuo, S.A. Nayfeh, Low order continuous-time filters for approximation of the ISO 2631-1 human vibration sensitivity weightings, J. Sound Vib. 265 (2003) 459–465.
[23] V.S. Deshpande, P.D. Shendge, S.B. Phadke, Nonlinear control for dual objective active suspension systems, IEEE Trans. Intell. Transport. Syst. 18 (3) (2017) 656–665.
[24] M. Corless, G. Leitmann, Continuous state feedback guaranteeing uniform ultimate boundedness for uncertain dynamic systems, IEEE Trans. Automat. Contr. 26 (5) (1981) 1139–1144.
[25] A. Akbari, B. Lohmann, Output feedback H-∞/GH 2 preview control of active vehicle suspensions: a comparison study of LQG preview, Veh. Syst. Dyn. 48 (12) (2010) 1475–1494.
[26] S.B.A. Kashem, M. Ektesabi, R. Nagarajah, Comparison between different sets of suspension parameters and introduction of new modified skyhook control strategy incorporating varying road condition, Veh. Syst. Dyn. 50 (7) (2012) 1173–1190.
[27] ISO-8608, Mechanical Vibration-road Surface Profiles-reporting of Measured Data, ISO, Geneva.
[28] F. Tyan, Y.-F. Hong, S.-H. Tu, W.S. Jeng, Generation of random road profiles, J. Adv. Eng. 4 (2) (2009) 1373–1378.
[29] Quanser, Active Suspension System: User Manual, Quanser Corporation.
[30] E.R.P. da Silva, E. Assuncao, M.C.M. Teixeira, R. Cardim, Robust controller implementation via state-derivative feedback in an active suspension system subjected to fault, in: Control and Fault-tolerant Systems (SysTol), 2013 Conference on, IEEE, 2013, pp. 752–757.

[31] S. Formentin, A. Karimi, A data-driven approach to mixed-sensitivity control with application to an active suspension system, IEEE Trans. Ind. Inf. 9 (4) (2013) 2293–2300.
[32] H.O. Ozer, Y. Hacioglu, N. Yagiz, High order sliding mode control with estimation for vehicle active suspensions, Trans. Inst. Meas. Contr. (2017) 1457–1470.
[33] U. Rashid, M. Jamil, S.O. Gilani, I.K. Niazi, LQR based training of adaptive neuro-fuzzy controller, in: Advances in Neural Networks, Springer, 2016, pp. 311–322.
[34] Y. Taskin, Y. Hacioglu, N. Yagiz, Experimental evaluation of a fuzzy logic controller on a quarter car test rig, J. Braz. Soc. Mech. Sci. Eng. 39 (7) (2017) 2433–2445.
[35] W. He, X. He, M. Zou, H. Li, PDE model-based boundary control design for a flexible robotic manipulator with input backlash, IEEE Trans. Contr. Syst. Technol. (2018) 1–8, https://doi.org/10.1109/TCST.2017.2780055.